Understanding the sources of the X-ray background: VLT identifications in the *Chandra*/*XMM-Newton* Deep Field South

G. HASINGER[1], J. BERGERON[2], V. MAINIERI[3], P. ROSATI[3], G. SZOKOLY[1] and the CDFS Team

[1]Max-Planck-Institut für Extraterrestrische Physik, Garching, Germany
[2]Institut d'Astrophysique, Paris, France
[3]European Southern Observatory, Garching, Germany

1. Introduction

Deep X-ray surveys indicate that the cosmic X-ray background (XRB) is largely due to accretion onto supermassive black holes, integrated over cosmic time. In the soft (0.5-2 keV) band more than 90% of the XRB flux has been resolved using 1.4 Msec observations with *ROSAT* (Hasinger et al., 1998) and recently 1-2 Msec *Chandra* observations (Rosati et al., 2002; Brandt et al., 2002) and 100 ksec observations with *XMM-Newton* (Hasinger et al., 2001). In the harder (2-10 keV) band a similar fraction of the background has been resolved with the above *Chandra* and *XMM-Newton* surveys, reaching source densities of about 4000 deg^{-2}. Surveys in the very hard (5-10 keV) band have been pioneered using BeppoSAX, which resolved about 30% of the XRB (Fiore et al., 1999). *XMM-Newton* and *Chandra* have now also resolved the majority (60-70%) of the very hard X-ray background.

Optical follow-up programs with 8-10m telescopes have been completed for the *ROSAT* deep surveys and find predominantly Active Galactic Nuclei (AGN) as counterparts of the faint X-ray source population (Schmidt et al., 1998; Lehmann et al., 2001) mainly X-ray and optically unobscured AGN (type-1 Seyferts and QSOs) and a smaller fraction of obscured AGN (type-2 Seyferts). The X-ray observations have so far been about consistent with population synthesis models based on unified AGN schemes (Comastri et al., 1995; Gilli, Salvati & Hasinger, 2001), which explain the hard spectrum of the X-ray background by a mixture of absorbed and unabsorbed AGN, folded with the corresponding luminosity function and its cosmological evolution. According to these models, most AGN spectra are heavily absorbed and about 80% of the light produced by accretion will be absorbed by gas and dust (Fabian et al., 1998). However, these models are far from unique and contain a number of hidden assumptions, so that their predictive power remains limited until complete samples of spectroscopically classified hard X-ray sources are available. In particular they require a substantial contribution of high-luminosity obscured X-ray sources (type-2 QSOs), which so far have only scarcely been detected. The cosmic history of obscuration and its potential depend-

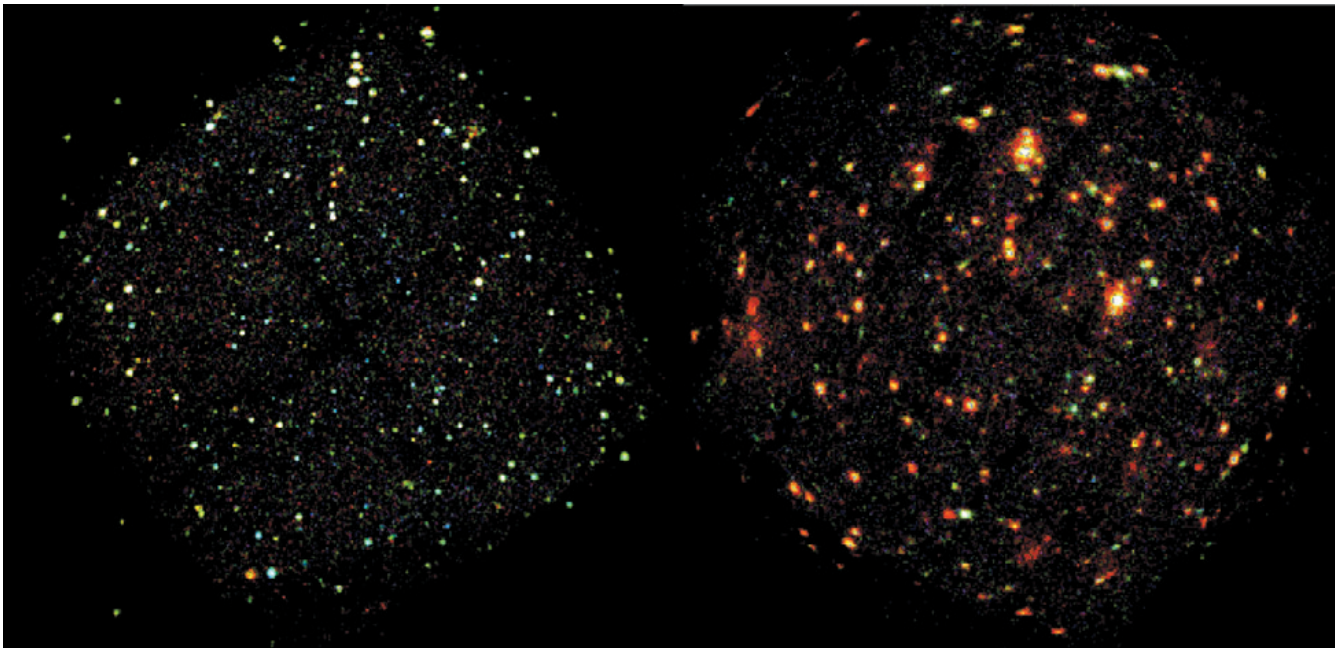

Figure 1: left: Composite image of the Chandra Deep Field South of 940 ks (pixel size=0.984", smoothed with a r=1" Gaussian). The image was obtained combining three energy bands: 0.3-1 keV, 1-3 keV, 3-7 keV (respectively red, green and blue). Right: Similar image for the 370 ksec dataset from XMM–Newton, roughly to the same scale. The three energy bands are: 0.5-2 keV, 2-4.5 keV, and 4.5-10 keV, respectively. A few diffuse reddish (i.e. soft) sources, associated with groups of galaxies can be seen. The color intensity is derived from the net counts and has not been corrected for vignetting.

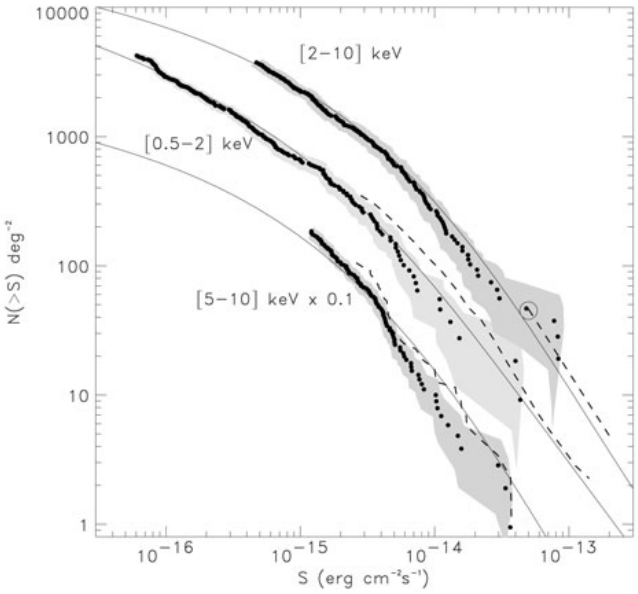

Figure 2: Number counts (logN – logS) in the soft (0.5-2 keV), hard (2-10keV) and very hard (5-10 keV) bands from the 1 Megasec observations of the CDFS (Rosati et al., 2002). The grey regions refer to statistical and systematic errors. Solid lines are predictions from model B by Gilli, Salvati & Hasinger (2001).

ence on intrinsic source luminosity remain completely unknown. Gilli et al. e.g. assumed strong evolution of the obscuration fraction (ratio of type-2/type-1 AGN) from 4:1 in the local universe to much larger covering fractions (10:1) at high redshifts (see also Fabian et al., 1998). The gas to dust ratio in high-redshift, high-luminosity AGN could be completely different from the usually assumed galactic value due to sputtering of the dust particles in the strong radiation field (Granato et al., 1997). This might provide objects which are heavily absorbed at X-rays and unobscured at optical wavelengths.

After having understood the basic contributions to the X-ray background, the general interest is now focussing on understanding the physical nature of these sources, the cosmological evolution of their properties, and their role in models of galaxy evolution. We know that basically every galaxy with a spheroidal component in the local universe has a supermassive black hole in its centre (Gebhardt et al., 2000). The luminosity function of X-ray selected AGN shows strong cosmological density evolution at redshifts up to 2, which goes hand in hand with the cosmic star formation history (Miyaji et al., 2000). At the redshift peak of optically selected QSO around z = 2.5 the AGN space density is several hundred times higher than locally, which is in line with the assumption that most galaxies have been active in the past and that the feeding of their black holes is reflected in the X-ray background. While the comoving space density of optically and radio-selected QSO has been shown to decline significantly beyond a redshift of 2.5 (Schmidt, Schneider & Gunn, 1995; Shaver et al., 1996), the statistical quality of X-ray selected AGN high-redshift samples still needs to be improved (Miyaji et al., 2000). The new *Chandra* and *XMM-Newton* surveys are now providing strong additional constraints here.

Optical identifications for the deepest *Chandra* and *XMM-Newton* fields are still in progress, however a mixture of obscured and unobscured AGN with an increasing fraction of obscuration at lower flux levels seems to be the dominant population in these samples too (Barger et al., 2001; Rosati et al., 2002; Stern et al., 2002; Szokoly et al., 2002; see below). Interestingly, first examples of the long-sought class of high-redshift, high-luminosity, heavily obscured active galactic nuclei (type-2 QSO) have been detected in deep *Chandra* fields (Norman et al., 2002; Stern et al., 2002) and in the *XMM-Newton* deep survey in the Lockman Hole field (Lehmann et al., 2002).

In this paper we give an update on the optical identification work in the *Chandra* Deep Field South, which thanks to the efficiency of the VLT has progressed furthest among the deepest X-ray surveys.

2. The *Chandra* Deep Field South (CDFS)

The *Chandra* X-ray Observatory has performed deep X-ray surveys in a number of fields with ever increasing exposure times (Mushotzky et al., 2000; Hornschemeier et al., 2000, Giacconi et al., 2001) and has completed a 1 Msec exposure in the *Chandra* Deep Field South (CDFS, Rosati et al., 2002) and a 2 Msec exposure in the Hubble Deep Field North (HDF-N, Brandt et al., 2002). The Megasecond dataset of the CDFS (500 ksec from R. Giacconi's guaranteed time, augmented by 500 ksec director's discretionary time) is the result of the coaddition of 11 individual *Chandra* ACIS-I exposures with aimpoints only a few arcsec from each other. The nominal centre of the CDFS is α = 03^{h}32^{m}28.0^s, δ = –27°48′30″ (J2000). This field was selected in a patch of the southern sky characterized by a low galactic neutral hydrogen column density $N_H = 8 \times 10^{19}$ cm^{-2} and a lack of bright stars (see Rosati et al., 2002).

In Figure 1 (left), we show the colour composite *Chandra* image of the CDFS. This was constructed by combining images (smoothed with a Gaussian with r = 1″ in three bands (0.3–1 keV, 1–3 keV, 3–7 keV), which contain approximately equal numbers of photons from detected sources. Blue sources are those undetected in the soft (0.5–2 keV) band, most likely due to intrinsic absorption from neutral hydrogen with column densities $N_H > 10^{22}$ cm^{-2}. Very soft sources appear red. A few extended low surface brightness sources are also readily visible in the image.

The CDFS was also observed with *XMM-Newton* for a total of ~500 ksec in July 2001 and January 2002 in guaranteed observation time (PI: J. Bergeron). Due to high background conditions some data were lost and a total of ~ 370 ksec has finally been accumulated. The colour composite image of the *XMM-Newton* dataset is shown in Figure 1 (right), smoothed with a Gaussian with r = 5″, using three energy bands (0.5–2 keV, 2–4.5 keV, 4.5–10 keV), thus harder than the *Chandra* image. The analysis of the *XMM-Newton* data is still ongoing, but we can conclude that the hard band sensitivity (5–10 keV) is comparable to the Megasecond *Chandra* image. The EPIC cameras have a larger

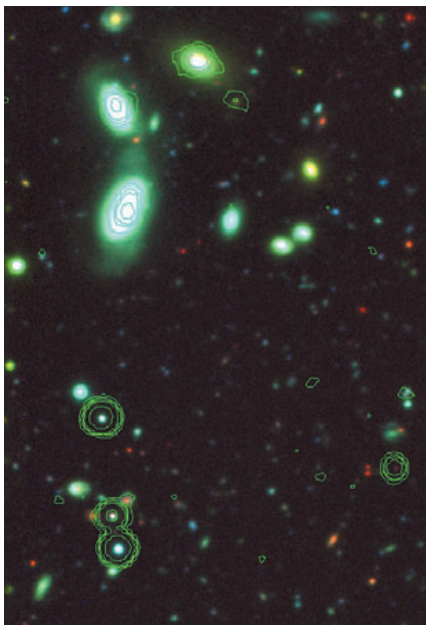

Figure 3: Cutout of a part of the CDFS. A deep FORS R-image has been combined with the EIS WFI B-image and the GOODS ISAAC K-image. X-ray contours are overplotted on the optical/NIR data. The image shows diffuse X-ray emission for the bright galaxies.

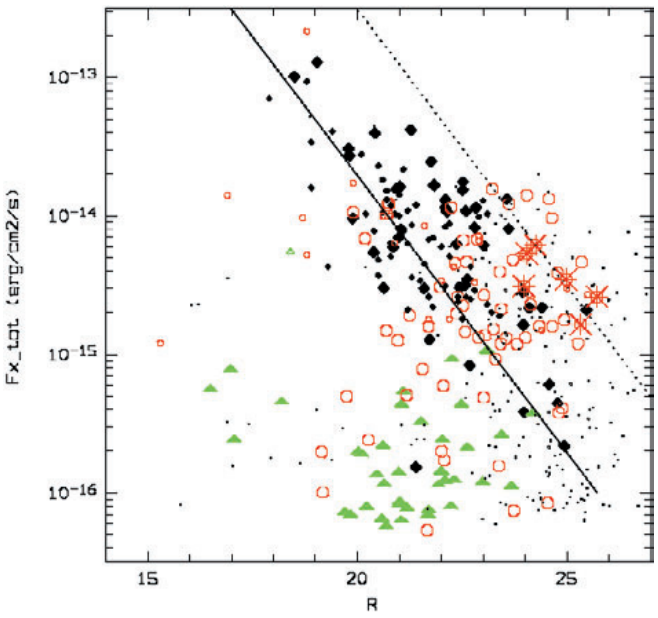

Figure 4: X-ray flux versus R-band magnitude for the CDFS sources (large symbols) and the ultra-deep ROSAT survey in the Lockman Hole (small symbols). Objects are coloured according to their X-ray/optical classification (see below): filled black diamonds correspond to type-1 AGN, open red hexagons to type-2 AGN and green triangles to galaxies. The large asterisks indicates type-2 QSOs (see text). Small dots refer to spectroscopically unidentified CDFS sources, the brighter ones of which have photometric redshifts. The solid line corresponds to an X-ray to optical flux ratio of 1, the dashed line is at an optical limit 3 magnitudes fainter.

field-of-view than ACIS, and a number of new diffuse sources are detected just outside the *Chandra* image. X-ray spectroscopy of a large number of sources will ultimately be very powerful with *XMM-Newton* (see Mainieri et al., 2002 for the Lockman Hole).

In Figure 2 (from Rosati et al., 2002), we show the *Chandra* cumulative number counts in three bands: soft, hard and very hard (5–10 keV). The logN-logS distribution shows a significant cosmological flattening in the softer bands, while in the very hard band it is still relatively steep, indicating that those surveys have not yet sampled the redshifts where the strong cosmological evolution of the sources saturates.

3. Optical identifications in the CDFS

Our primary optical imaging was obtained using the FORS1 camera on the ANTU (UT-1 at VLT) telescope. The R band mosaics from these data cover 13.6′ × 13.6′ to depths between 26 and 26.7 (Vega magnitudes). These data do not cover the full CDFS area and must be supplemented with other observations. The ESO Imaging Survey (EIS) has covered this field to moderate depths in several bands (Arnouts et al. 2001; Vandame et al. 2001). The EIS data have been obtained using the Wide Field Imager (WFI) on the ESO-MPG 2.2 meter telescope at La Silla.

Figure 3 shows *Chandra* X-ray contours in a selected area of the CDFS superposed on a deep BRK multicolour image. The positioning is better than 0.5″ and we readily identify likely optical counterparts in 85% of the cases (78% for the shallower WFI data). Note the very red object in the lower right, which is only detected at K. Figure 4 shows the classical correlation between optical (R-band) magnitude and X-ray flux of the CDFS-objects in comparison with the deepest *ROSAT* survey in the Lockman Hole (Lehmann et al., 2001). Generally the 0.5-2 keV flux is given, however, for *Chandra* sources not detected in the soft band, the 2-10 keV flux is given. Sources are marked according to their optical classification (see below). The *Chandra* data extend the previous ROSAT range by a factor of ~40 in flux and to substantially fainter optical magnitudes. While the bulk of the type-1 AGN population still follows the general correlation along a constant f_X/f_{opt} line, the type-2 AGN cluster at higher X-ray to optical flux ratios. There is also a new population of normal galaxies showing up at significantly brighter optical magnitudes.

4. VLT optical spectroscopy

Optical spectroscopy has been carried out in ~11 nights with the ESO Very Large Telescope (VLT) in the time frame April 2000 - December 2001, using deep optical imaging and low resolution multiobject spectroscopy with the FORS instruments with individual exposure times ranging from 1-5 hours. Some preliminary results including the VLT optical spectroscopy have already been presented (Norman et al., 2002; Rosati et al., 2002). The complete opti-

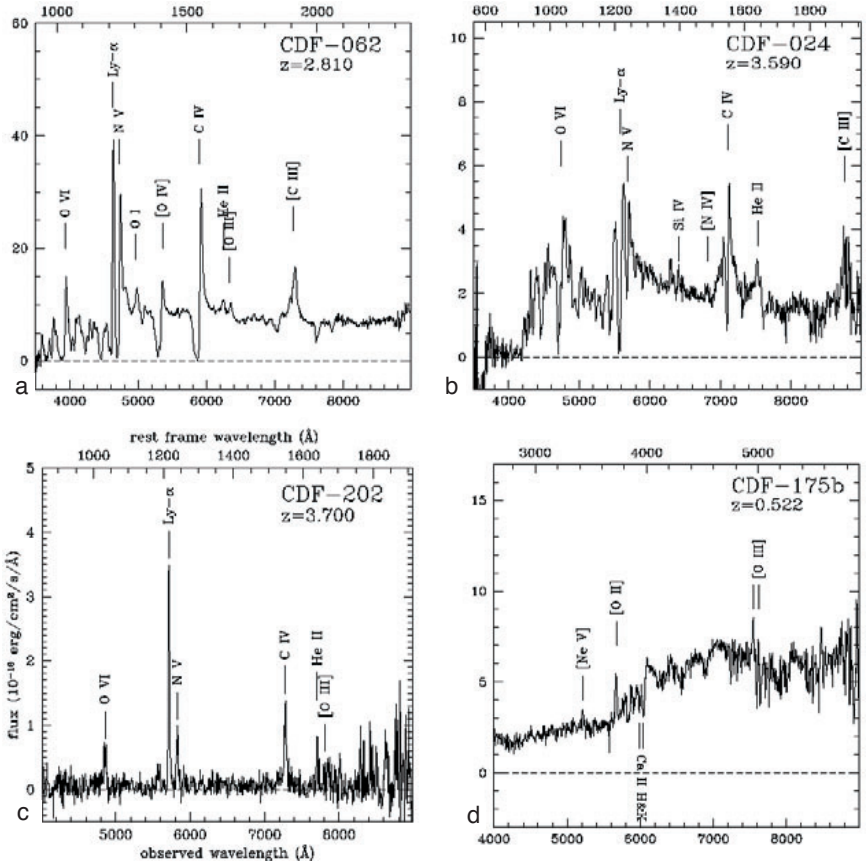

Figure 5: Optical spectra of some selected CDFS sources obtained using multiobject-spectroscopy with FORS at the VLT (Szokoly et al., 2002). a: broad absorption line (BAL) QSO CDFS-062 at z=2.822 (see also Giacconi et al., 2001); b: high-redshift QSO CDFS-024 at z=3.605, showing strong absorption lines; c: QSO-2 CDFS-202 at z=3.700 (see Norman et al., 2002); d: Seyfert-2 CDFS-175b at z=0.522, showing a weak high excitation line of [NeV].

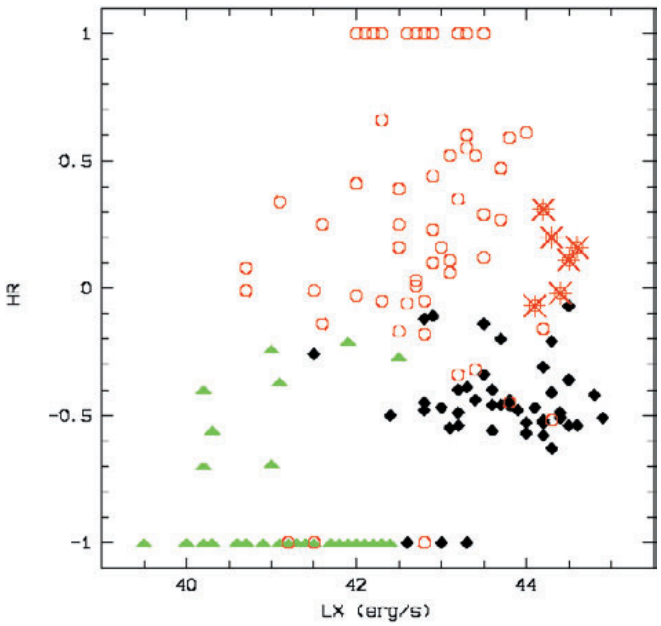

Figure 6: Hardness ratio versus rest frame luminosity in the total 0.5–10 keV band. Symbols as in Figure 4. A critical density universe with $H_0 = 50$ km s^{-1} Mpc^{-1} has been adopted. Luminosities are not corrected for possible intrinsic absorption.

cal spectroscopy will be published in Szokoly et al. (2002). Figure 5 shows examples of four VLT spectra of sources with X-ray absorption. The upper two spectra show high-redshift QSOs with restframe-UV absorption features (BAL or mini-BAL QSOs), which both show some indication of intrinsic absorption in their X-ray spectra. The object in the lower left is the famous, highest redshift type-2 QSO detected in the CDFS with heavy X-ray absorption and a ~7 keV Fe-line in the QSO rest frame (Norman et al., 2002). The spectrum in the lower right shows a Seyfert-2 galaxy with heavy X-ray absorption and an AGN-type luminosity. The latter spectrum is characteristic for the bulk of the detected galaxies, which show either no or very faint high excitation lines indicating the AGN nature of the object, so that we have to resort to a combination of optical and X-ray diagnostics to classify them as AGN (see below). Redshifts could be obtained so far for 169 of the 346 sources in the CDFS, of which 123 are very reliable (high quality spectra with 2 or more spectral features), while the remaining optical spectra contain only a single emission line, or are of lower S/N.

For objects fainter than R=24 reliable redshifts can be obtained if the spectra contain strong emission lines. For the remaining optically faint objects we have to resort to photometric redshift techniques. Nevertheless, for a subsection of the sample at off-axis angles smaller than 8 arcmin we obtain a spectroscopic completeness of about 60%.

5. Optical and X-ray classification

Type-1 AGN (Seyfert-1 and QSOs) can be often readily identified by the broad permitted emission lines in their optical spectra. Luminous Seyfert-2 galaxies show strong forbidden emission lines and high-excitation lines indicating photoionization by a hard continuum source. However, already in the spectroscopic identifications of the *ROSAT* Deep Surveys it became apparent, that an increasing fraction of faint X-ray selected AGN shows a significant, sometimes dominant contribution of stellar light from the host galaxy in their optical spectra, depending on the ratio of optical luminosity between nuclear and galaxy light (Lehmann et al., 2001). If an AGN is much fainter than its host galaxy it is not possible to detect it optically. Many of the counterparts of the faint X-ray sources detected by *Chandra* and *XMM-Newton* show optical spectra dominated by their host galaxy and only a minority have clear indications of an AGN nature (see also Barger et al., 2001). In these cases, the X-ray emission could still be dominated by the active galactic nucleus, while a contribution from stellar and thermal processes (hot gas from supernova remnants, starbursts and thermal halos, or a population of X-ray binaries) can be important as well.

Therefore X-ray diagnostics in addition to the optical spectroscopy can be crucial to classify the source of the X-ray emission. AGN have typically (but not always!) X-ray luminosities above 10^{42} erg s^{-1} and power law spectra, often with significant intrinsic absorption. Local, well-studied starburst galaxies have X-ray luminosities typically below 10^{42} erg s^{-1} and very soft X-ray spectra. Thermal haloes of galaxies and the intergalactic gas in groups can have higher X-ray luminosities, but have soft spectra as well. The redshift effect in addition helps the X-ray diagnostic, because soft X-ray spectra appear even softer already at moderate redshift, while the typical AGN power law spectra appear harder over a very wide range of redshifts.

Following Rosati et al (2002), we show in Figure 6 the hardness ratio as a function of the luminosity in the 0.5–10 keV band for 165 sources for which we have optical spectra and rather secure classification (Szokoly et al. in preparation). The hardness ratio is defined as $HR = (H–S)/(H+S)$ where H and S are the net count rates in the hard (2–7 keV) and the soft band (0.5–2 keV), respectively. The X-ray luminosities are not corrected for internal absorption and are computed in a critical density universe with $H_0 = 50$ km s^{-1} Mpc^{-1}.

Different source types are clearly segregated in this plane. Type-1 AGNs (black diamonds) have luminosities typically above 10^{42} erg s^{-1}, with hardness ratios in a narrow range around *HRj*–0.5. This corresponds to an effective G = 1.8, commonly found in type-1 AGN. Type-2 AGN are skewed towards significantly higher hardness ratios (HR > 0), with (absorbed) luminosities in the range $10^{41–44}$ erg s^{-1}. Direct spectral fits of the *XMM-Newton* and (some) *Chandra* spectra clearly indicate that these harder spectra are due to neutral gas absorption and not due to a flatter intrinsic slope (see Mainieri et al., 2002). Therefore the unabsorbed, intrinsic luminosities of type-2 AGN would fall in the same range as those of type-1's.

In Figure 6, we also indicate the type-2 QSOs (asterisks), the first one of which was discovered in the CDFS (Norman et al. 2002). In the meantime, more examples have been found in the CDFS and elsewhere (e.g. Stern et al. 2002). It is interesting to note that no high-luminosity, very hard sources exist in this diagram. This is a selection effect of the pencil beam surveys: due to the small solid angle, the rare high luminosity sources are only sampled at high redshifts, where the absorption cut-off of type-2 AGN is redshifted to softer X-ray energies. Indeed, the type-2 QSOs in this sample are the objects at $L_X > 10^{44}$ erg s^{-1} and $HR > –0.2$. The type-1 QSO in this region of the diagram is a BAL QSO with significant intrinsic absorption.

About 10% of the objects have optical spectra of normal galaxies (marked with triangles), luminosities below 10^{42} erg s^{-1} and very soft X-ray spectra (several with $HR = –1$), as expected in the case of starbursts or thermal halos. Those at $L_X < 10^{41.5}$ erg s^{-1} and HR larger than –0.7 are at particularly low redshifts. However, a separate subset has harder spectra ($HR > –0.5$), and luminosities $>10^{41}$ erg s^{-1}. In these galaxies the X-ray emission is likely due to a mixture of low level AGN activity and a population of low mass X-ray binaries (see also Barger et al., 2001). Therefore the deep *Chandra* and *XMM-Newton* surveys detect for the first time the population of normal starburst

galaxies out to intermediate redshifts (Mushotzky et al., 2000; Giacconi et al., 2001; Lehmann et al., 2002). These galaxies might become an important means to study the star formation history in the universe completely independently from optical/UV, sub-mm or radio observations.

6. The redshift distribution

Figure 7 shows the optical magnitudes of the spectroscopically identified CDFS sources as a function of redshift. There is a segregation between type-1 and type-2 AGN at high redshifts, most likely because the optical light from type-1 AGN contains a significant non-thermal contribution in addition to the host galaxy. Reliable redshifts can be obtained at the VLT typically for objects with R<25.5, however, some incompleteness already sets in around R=23. The CDFS has a spectroscopic completeness of about 60%, which is mainly caused by the fact that about 40% of the counterparts are optically too faint to obtain reliable spectra. Photometric redshift estimates of the remainder of the sources indicate a redshift distribution similar to the spectroscopic one.

The completeness of 60% therefore allows us to compare the redshift distribution with predictions from X-ray background population synthesis models (Gilli, Salvati & Hasinger 2001), based on the AGN X-ray luminosity function and its evolution as determined from the *ROSAT* surveys (Miyaji et al., 2000), which predict a maximum at redshifts around z = 1.5. It is interesting to note, that contrary to these expectations, the bulk of the CDFS objects are found at redshifts below 1. The redshift distribution peaks at $z \sim 0.7$, even if the normal star forming galaxies in the sample are removed. This clearly demonstrates that the population synthesis models will have to be modified to incorporate different luminosity functions and evolutionary scenarios for intermediate-redshift, low-luminosity AGN.

In Figure 7 there is an interesting accumulation of redshifts in the range z = 0.6–0.8. We obviously have discovered two large-scale structures at redshifts z = 0.66 and z = 0.73, respectively, which are made up of type-1 and type-2 AGN as well as normal galaxies in roughly the same proportion as observed in the field. The objects in these redshift spikes are distributed across a large fraction of the field, so that they are probably sheet-like structures. At least one of them (at z = 0.73) is also seen in the K-band selected galaxy survey of Cimatti et al. (2002) and corresponds to several X-ray clusters in the field. It will be interesting to study the correlation of active galaxies to field galaxies in these sheets and to try to determine the role that galaxy mergers play in the triggering of the AGN activity. Finally, there may be a relation between the surprisingly low redshift of the bulk of the *Chandra* sources, the existence of the sheets at the same redshift and the strongly evolving population of dusty starburst galaxies inferred from the ISO mid-infrared surveys (Franceschini et al., 2002).

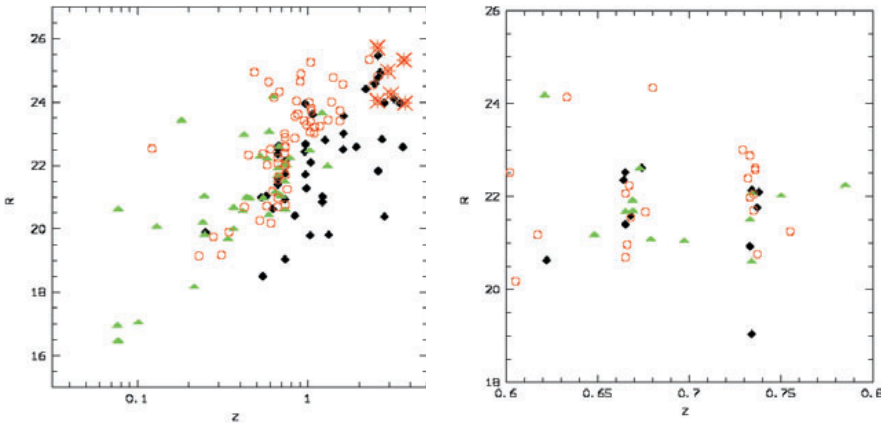

Figure 7: Left: Optical magnitudes as a function of redshift for the CDFS objects. Symbols are as in Figure 4. An accumulation of objects in two redshift bins around z=0.7 (enlarged in the right figure) is due to a large scale structure in the CDFS.

By no means does the CDFS redshift distribution confirm the prediction by Haiman & Loeb (1999), that a large number (~100) QSO at redshifts larger than 5 should be expected in any ultra deep *Chandra* survey. The highest redshift in the CDFS thus far is 3.7, while there are two objects at z = 4.4 and z = 5.2, respectively, in the HDF-N (Brandt et al., 2002) and one QSO at z = 4.5 in the Lockman Hole (Schneider et al. 1998). This suggests a cut-off of the X-ray selected QSO space density at high redshift.

7. Summary and outlook

Deep X-ray surveys have shown that the cosmic X-ray background (XRB) is largely due to accretion onto supermassive black holes, integrated over cosmic time. The findings are consistent with the notion that most larger galaxies contain black holes which have been active in the past. However, the characteristic hard spectrum of the XRB can only be explained if most AGN spectra are heavily absorbed (Comastri et al. 1995). Thus about 80-90% of the light produced by accretion must be absorbed by gas and dust clouds, which may reside in nuclear starburst regions that feed the AGN (Fabian et al., 1998).

The star formation history has been determined in the last years based on optical and UV measurements (Steidel et al., 1999). However, deep submillimeter surveys with SCUBA have revealed the existence of a large population of hitherto undetected dust-enshrouded galaxies (e.g. Hughes et al. 1998), which may provide the dominant contribution to the star formation rate at higher redshifts. The spectral shape of the X-ray background may be related to the dust obscuration of the far-infrared sources, which are believed to be the high-z equivalents of the ultra luminous IR galaxies (ULIRGs). For some ULIRGs the presence of heavily obscured AGN has been inferred by *BeppoSAX* (e.g. Vignati et al. 1999). Therefore a relation between the faint X-ray and far-infrared source populations is expected. Indeed, a large fraction of the faint hard *Chandra* and *XMM-Newton* sources have infrared counterparts in deep ISOCAM images (Fadda et al., 2002, Alexander et al., 2002) and the redshift distribution of faint X-ray sources and Mid-IR sources is similar (see above).

The so-far deepest X-ray and SCUBA observations (Hornschemeier et al., 2000) did pick up only very few common objects. Even deeper X-ray images in conjunction with deep surveys at the peak wavelength of the far-infrared background e.g. with SIRTF, are therefore required. The *Chandra* Deep Field South has been selected as one of the deep fields in the SIRTF legacy programme “Great Observatories Origins Deep Survey” (GOODS). GOODS will produce the deepest observations with the SIRTF IRAC instrument at 3.6–8 μm and with the MIPS instrument at 24 μm and together with the Chandra data provide the necessary depth and statistics to finally establish the FIR/X-ray relation.

In addition to the data described here, a large number of supporting observations across a wide range of the electromagnetic spectrum are being carried out or planned. We have proposed to complement the already existing *Chandra* Megasecond observations with two 500 ksec ACIS-I pointings to homogenize and increase the exposure in the GOODS are a to 2 Msec. Three small regions in the CDFS have already been observed with HST, which provides excellent morphology of the AGN host galaxies and photometry for the

faintest optical counterparts (Koekemoer et al., 2002). The whole CDFS will soon be covered by an extensive set of pointings with the new Advanced Camera for Surveys (ACS) in BVIz to "near HDF" depth. Following up the deep EIS survey in the CDFS, ESO has started a large program to image the GOODS area with the VLT to obtain deep JHKs images in some 32 ISAAC fields. The first imaging data covering the central 50 arcmin^2 have recently been made public. Optical spectroscopy across the whole field will be obtained with very high efficiency using VIRMOS on the VLT.

The multiwavelength coverage of the field will be complemented by deep radio data from the VLA at 6 cm (already obtained) and ATCA at 20 cm. The CDFS/GOODS will therefore ultimately be one of the patches in the sky providing a combination of the widest and deepest coverage at all wavelengths and thus a legacy for the future.

References

Alexander D.M., Aussel H., Bauer F.E., et al., 2002, ApJ 568, L85

Arnouts S., Vandame B., Benoist C., et al., 2001, A&A. 379, 740

Barger, A. J., Cowie, L. L., Mushotzky, R. F., Richards, E. A., 2001, AJ 121, 662

Brandt W.N., Alexander D.M., Bauer, F.E., Hornschemeier A.E., 2002, astro-ph/0202311

Cimatti, A., Daddi E., Mignoli M., et al., 2002, A&A 381, L.68

Comastri, A.; Setti, G.; Zamorani, G.; Hasinger, G., 1995, A&A 296, 1

Fabian A.C., Barcons X., Almaini O., Iwasawa K., 1998, MNRAS 297, L11

Fadda D., Flores H., Hasinger G., 2002, A&A 383, 838Fiore F., La Franca F., Giommi P., et al., 1999, MNRAS 306, 55

Franceschini A., Fadda D., Cesarsky C., et al., 2002, ApJ 568, 470

Gebhardt K., Bender R., Bower G., et al., 2000, ApJ 539, 13Giacconi, R., Rosati P., Tozzi P., et al., 2001, ApJ 551, 624

Gilli, R., Salvati, M., Hasinger, G., 2001, A&A 366, 407

Granato G.L., Danese L., Francheschini A., 1997, ApJ 486, 147

Haiman, Z. & Loeb A., 1999, ApJ 519, 479

Hasinger, G., Burg, R., Giacconi, R., et al., 1998, A&A 329, 482

Hasinger, G., Altieri, B., Arnaud, M., et al., 2001, A&A 365, 45

Hornschemeier, A.E., Brandt, W.N., Garmire, G.P., et al., 2000, ApJ 541

Hughes D.H., Serjeant S., Dunlop J., et al., 1998, Nature 394, 241

Koekemoer A.M., Grogin N.A., Schreier E.J., 2002, ApJ 567, 657

Lehmann, I., Hasinger, G., Schmidt, M., et al., 2001, A&A 371, 833

Lehmann I., Hasinger G., Murray S.S, Schmidt M., 2002, astro-ph/0109172

Mainieri V., Bergeron J., Rosati P., et al., 2002, astro-ph/0202211

Miyaji, T., Hasinger, G., Schmidt, M., 2000, A&A 353, 25

Mushotzky, R.F., Cowie L.L., Barger, A.J., Arnaud, K.A., 2000, Nature 404, 459

Norman C., Hasinger G., Giacconi R., et al. 2002, ApJ 571, 218

Rosati P., Tozzi P., Giacconi R., et al., 2002, ApJ 566, 667

Schmidt, M., Schneider, D.P. \& Gunn J.E., 1995, AJ 114, 36

Schmidt, M., Hasinger, G., Gunn, J.E., et al., 1998, A&A 329, 495

Schneider, D.P., Schmidt, M., Hasinger, G., et al., 1998, AJ 115, 1230

Shaver P.A. et al., 1996, Nature 384, 439

Steidel C.C., Adelberger K.L., Giavalisco M., Dickinson M., Pettini M., 1999, ApJ 519, 1

Stern D., Moran E.C., Coil A.L., et al., 2002, ApJ 568, 71

Szokoly, G., Hasinger G., Rosati, P. et al., 2002 (in prep.)

Vandame et al. 2001, astro-ph/0102300

Vignati P., Molendi S., Matt G., et al., 1999, A&A 349, L57

Using color-magnitude diagrams and spectroscopy to derive star formation histories: VLT observations of Fornax

CARME GALLART[1], Andes Prize Fellow, Departamento de Astronomía, Universidad de Chile, and Department of Astronomy, Yale University
ROBERT ZINN, Department of Astronomy, Yale University
FREDERIC PONT[2], Departamento de Astronomía, Universidad de Chile
EDUARDO HARDY, National Radio Astronomy Observatory
GIANNI MARCONI, European Southern Observatory
ROBERTO BUONANNO, Osservatorio Astronomico di Roma

1. Star formation and chemical enrichment histories of the Milky Way satellites

During the last decade, the varied star formation histories of the dSph galaxies satellites of the Milky Way have been revealed to us in detail, dramatically changing our perception from the early idea that they were predominantly old systems. Some hints on the presence of, at least, an intermediate-age population had been provided previously by the peculiarity of the variable star populations of dSph galaxies (Norris & Zinn 1975) and the discovery of Carbon stars in Fornax (Demers & Kunkel 1979; Aaronson & Mould 1980), Carina (Cannon, Niss & Norgaard-Nielsen 1981) and other dSph (Aaronson, Olszewski & Hodge 1983). However, only in the last few years have these intermediate-age populations been shown beautifully in the wide-field, extremely deep CMDs of a number of dSph galaxies. There is the extreme case of Leo I (Caputo et al. 1999; Gallart et al. 1999a,b), which has formed over 80% of its stars from 6 to 1 Gyr ago, and the intermediate cases of Carina (Smecker-Hane et al. 1996; Hurley-Keller et al. 1998; Castellani et al. 2001) and Fornax (Stetson et al. 1997; Buonanno et al. 1999), with prominent intermediate-age populations. There are also predominantly old systems like Draco (Aparicio et al. 2001) and Ursa Minor (Carrera et al. 2002).

These CMDs offer qualitative first glances at the star formation histories (e.g. in the case of Carina, one can see that there have been three major events of star formation), but their quantitative determination requires a detailed comparison of the distribution of stars in the CMD with that predicted by model CMDs. CMDs reaching the old main-sequence turnoffs are particularly useful for these comparisons because there are few uncertainties in the theory for this stage of a star's life and there is less age-metallicity degeneracy. We have shown that with this method, it is possible to break the classical age-metallicity degeneracy in stellar populations for systems with low levels of metal enrichment like Leo I (Gallart et al. 1999b). However, in the case of a more complicated chemical

[1]Currently: Ramon y Cajal Fellow. Instituto de Astrofísica de Canarias.
[2]Currently: Observatoire de Genève.